

Behaviors of Surface Plasmon Coupled Light-Emitting Diodes Induced by Surface Ag Nanoparticles on Dielectric Interlayers

Chun-Han Lin · Chung-Hui Chen · Yu-Feng Yao ·
Chia-Ying Su · Pei-Ying Shih · Horng-Shyang Chen ·
Chieh Hsieh · Yang Kuo · Yean-Woei Kiang · C. C. Yang

Received: 23 November 2014 / Accepted: 20 January 2015 / Published online: 5 February 2015
© Springer Science+Business Media New York 2015

Abstract The enhanced surface plasmon (SP) coupling effects in a blue light-emitting diode (LED) with regularly patterned (REG) surface Ag nanoparticles (NPs) on a dielectric interlayer (DI) of a lower refractive index overgrown on p-GaN are demonstrated. Without a DI, the surface Ag NPs-induced SP coupling with the quantum wells (QWs) in the LED can lead to the increases of internal quantum efficiency and LED output intensity, the reduction of the external quantum efficiency droop effect, and the enhancement of modulation response. By adding a DI, the SP coupling effect is enhanced, resulting in the further improvements of all the aforementioned factors. We compare the SP coupling effects in the LEDs with REG Ag NPs on DIs to those of randomly distributed (RAN) Ag NPs previously reported. Although the variation trends of the localized surface plasmon (LSP) resonance peaks and hence the SP coupling behaviors of REG and RAN Ag NPs are similar, their LSP resonance strengths at the QW emission wavelength are different due

to their different spectral patterns of LSP resonance. In other words, although the REG Ag NPs can produce stronger collective LSP resonance with a narrower spectral width, the SP coupling effect depends mainly on the LSP resonance strength at the QW emission wavelength.

Keywords Surface plasmon · Light-emitting diode · Ag nanoparticle · Dielectric interlayer

Introduction

By fabricating a metal nanostructure on a light-emitting diode (LED), the induced surface plasmon (SP) coupling with the quantum wells (QWs) of the LED can create an alternative light emission channel and hence enhance the internal quantum efficiency (IQE) and LED output intensity [1–10]. Also, because of the significant decrease of the carrier density in the QWs during the SP coupling process, either effect of current overflow [11–13] or Auger recombination [14–16] in an LED is weakened, leading to the reduction of the efficiency droop effect [17–19]. Among the metals used for generating SP coupling, the resonance wavelength of an Au nanostructure is usually longer than the green range and its dissipation rate is higher, when compared with an Ag nanostructure. Meanwhile, the SP resonance of Al is usually limited to the UV range. For visible application, Ag is an optimized choice, particularly for SP-coupled blue and green LEDs. Both surface plasmon polariton (SPP) and localized surface plasmon (LSP) resonance can induce SP coupling effects in an LED. Although SPP generated on a smooth surface can also couple with a radiating dipole in a QW for emission enhancement, a momentum compensation scheme,

C.-H. Lin · C.-H. Chen · Y.-F. Yao · C.-Y. Su · P.-Y. Shih ·
H.-S. Chen · C. Hsieh · Y.-W. Kiang · C. C. Yang (✉)
Institute of Photonics and Optoelectronics, National Taiwan
University, No. 1, Section 4, Roosevelt Road, Taipei 10617, Taiwan
e-mail: ccycc@ntu.edu.tw

Y.-W. Kiang
e-mail: ywkiang@ntu.edu.tw

Y. Kuo
Department of Energy and Refrigerating Air-conditioning
Engineering, Tung Nan University, 152 Beishen Road, Section 3,
New Taipei City 22202, Taiwan

Y.-W. Kiang · C. C. Yang
Department of Electrical Engineering, National Taiwan University,
No. 1, Section 4, Roosevelt Road, Taipei 10617, Taiwan

such as a metal grating, to shift the SPP dispersion curve into the light cone can significantly enhance emission. However, for blue-green LEDs, the period of such a metal grating must be in the range of 100 nm [18]. It is either difficult or expensive to fabricate such a metal grating. On the other hand, the fabrication of a metal nanoparticle (NP) or a local metal nanostructure for generating LSP resonance can be a more practical approach for implementing an SP-coupled LED. In particular, the distribution of surface metal NPs on an LED is a simple and inexpensive method for fabricating an SP-coupled LED [20, 21].

Although the theoretical short-wavelength limit of LSP resonance on a small Ag NP in air can be as short as ~200 nm, by forming such an Ag NP on or inside GaN, the major LSP resonance feature (the dipole resonance mode) for coupling with a QW is always located in the yellow-red range because LSP resonance wavelength increases with surrounding refractive index. In this situation, the application to blue-green LEDs relies on the higher order LSP resonance modes, which are usually weaker and have high dissipation rates [22]. Therefore, for effective SP coupling in the blue-green range, a certain scheme must be designed for blue-shifting the major LSP resonance feature into the blue-green range. Generally, the LSP resonance feature is blue shifted when the size of a metal NP is reduced. However, it has been numerically shown that the SP coupling effect of a single metal NP is reduced when its size becomes smaller [23]. In this situation, a higher planar metal NP density is required for achieving a strong SP coupling effect that may represent a technical difficulty. An alternative approach for blue-shifting the LSP resonance features of a metal NP is to place a dielectric interlayer (DI), which has a refractive index smaller than that of GaN (~2.4), on the top of an LED before depositing metal NPs. In the case of SPP with a flat metal/GaN interface, it has been theoretically and experimentally shown that by inserting a thin dielectric layer (such as SiO₂ of 1.5 in refractive index) between the metal and GaN layers, the SPP dissipation rate is reduced, the evanescent field intensity of SPP beyond a certain depth in GaN is increased, and the SPP density of state is decreased [23]. The combination of these factors can result in a further emission enhancement of QW through SPP coupling. In the case of LSP, although the SP coupling behavior after adding a DI can be different from that of SPP, it is expected that the smaller refractive index of the DI right below a metal NP can blue-shift its dipole resonance mode. In particular, the behavior of the substrate LPS mode, which has the major energy distributed around the interface between the metal NP and the substrate [21, 24], is expected to be sensitive to the refractive index change of the substrate. This substrate mode is the most important spatially distributed LSP mode coupling with the QWs in an SP-coupled LED. With a DI for blue-shifting the LSP resonance features, the overall LSP

resonance strength can be reduced. Nevertheless, because the emission wavelength of the QWs in an LED becomes closer to the LSP resonance peak, the SP coupling effect at the QW wavelength can become stronger. Recently, such an SP coupling behavior with a DI was demonstrated in a blue-emitting LED [19]. By inserting a SiO₂ or GaZnO thin layer as the DI between randomly distributed (RAN) Ag NPs and the p-GaN layer, the LSP resonance peak is blue shifted to become closer to the QW emission wavelength of the LED for enhancing the SP coupling effect. A lower refractive index or a larger thickness of the DI leads to a larger blue shift range.

InGaN/GaN QW LEDs have been used for the development of visible communications [25–28]. Combining with the function of general lighting, LEDs can be used for indoor short-range data transmission. In this regard, the modulation speed of an LED becomes an important issue. For increasing the modulation speed, a micro-LED of a small mesa has been developed for reducing the effective RC time constant in such a device [25]. Because the SP coupling process can increase the emission rate or carrier decay rate, the modulation speed of an SP-coupled LED is expected to be higher, when compared with a conventional LED.

Although the concept of blue-shifting the LSP resonance peak of surface metal NPs for enhancing SP coupling effect in the blue range by adding a DI has been briefly demonstrated [19], many details of such an SP coupling behavior have not been reported yet. In particular, because of the random size distribution in RAN metal NPs, the LSP resonance peaks of individual metal NPs are dispersed and hence the collective resonance peak is broad and weak. In this regard, the SP coupling effect of regularly patterned (REG) metal NPs is expected to be stronger near the collective LSP resonance peak, when compared with RAN metal NPs. In this paper, we first demonstrate the effects of adding a DI between the p-GaN layer and metal NPs in an SP-coupled LED with REG surface Ag NPs. Two DI materials of different refractive indices, including SiO₂ (~1.5 in refractive index) and GaZnO (~1.8 in refractive index), are used to observe the effect of varying the refractive index of the DI. Although GaZnO is a dielectric material in the optical spectral range, it is a good conductor under direct-current operation. The comparison between the REG Ag NP-induced SP-coupled LEDs with insulating SiO₂ and conductive GaZnO DIs can show us their different electrical properties. It is shown that with surface Ag NPs for producing significant LSP coupling, the IQE and LED output intensity is increased, photoluminescence (PL) decay time is shortened, efficiency droop effect is reduced, and modulation –3 dB frequency is increased. By adding the DIs, the variation ranges of these factors are increased following the same trends. The results of the LEDs with REG Ag NPs are compared to those with RAN surface Ag NPs when the same DI structures are added. Although the variation trends of LSP resonance peaks and hence SP

coupling behaviors of REG and RAN Ag NPs are similar, their LSP resonance strengths at a given QW emission wavelength can be different due to their different spectral patterns of LSP resonance. In this paper, we also compare the differences of SP coupling between LEDs with single and multiple QWs. In “Sample Structures and Fabrication Procedures” section of this paper, the sample structures and fabrication procedures are presented. The basic optical properties of those samples are shown in “Photoluminescence Characterization Results” section. Then, the characterization results of the LEDs with REG surface Ag NPs are reported in “Performances of the LEDs with Regularly Patterned Ag Nanoparticles” section. Next, the performances of the LEDs with RAN surface Ag NPs are briefly described in “Performances of the LEDs with Randomly Distributed Ag Nanoparticles” section for comparison. Discussions about various comparisons are made in “Discussions” section. Finally, the conclusions are drawn in “Conclusions” section.

Sample Structures and Fabrication Procedures

Four similar LED epitaxial structures are grown with metalorganic chemical vapor deposition on c-plane sapphire substrate. Each epitaxial structure consists of a 1- μm u-GaN layer, a 2- μm n-GaN layer, a QW structure (including a ~ 3 -nm InGaN well and ~ 10 nm u-GaN barriers on both sides in each period of QW), a 20-nm p-AlGaIn layer, and a p-GaN layer. The four LED epitaxial structures include the combinations of two p-GaN thicknesses at 50 and 120 nm and two QW period numbers at 1 and 5. The SP coupling behaviors with REG surface Ag NPs on various DI structures between the cases of thin and thick p-GaN and between the cases of single- and multiple-QW are to be compared. The QW emission wavelengths of all the four epitaxial structures are around 470 nm. Each LED epitaxial structure is used for fabricating five LED samples. Based on the epitaxial structure of thin p-GaN and single-QW, samples A1-E1 are processed without REG surface Ag NP (A1), with REG surface Ag NPs but without DI (B1), with REG surface Ag NPs and a SiO₂ layer of 3 nm in thickness as the DI (C1), with REG surface Ag NPs and a SiO₂ layer of 6 nm in thickness as the DI (D1), and with

REG surface Ag NPs and a GaZnO layer of 10 nm in thickness as the DI (E1), respectively. The same Ag NP and DI conditions are implemented on the epitaxial structure of thick p-GaN and single-QW for fabricating samples A1'-E1'. Then, the same Ag NP and DI conditions are implemented on the epitaxial structure of thin p-GaN and multiple-QW for fabricating samples A5-E5. Next, the same Ag NP and DI conditions are implemented on the epitaxial structure of thick p-GaN and multiple-QW for fabricating samples A5'-E5'. The detailed descriptions of the aforementioned 20 samples, including the average Ag NP sizes, are given in columns 2–5 of Table 1. The REG Ag NPs either on p-GaN or on a DI are patterned with nano-imprint lithography. First, a SiN (40 nm)/SiO₂ (40 nm) mask with triangularly patterned holes of 100 nm in hole diameter and 200 nm in pitch is formed through plasma-enhanced chemical vapor deposition and reactive ion etching [29]. In the case of a SiO₂ DI, SiO₂ is again deposited onto the patterned mask to form a SiO₂ layer of the designated thickness (3 or 6 nm) on the p-GaN surface at the bottom of a patterned hole. Then, an Ag layer of ~ 8 nm in thickness is deposited onto the mask. The Ag thickness inside the patterned holes is also ~ 8 nm. REG Ag NPs with a SiO₂ DI can be formed after a liftoff process through the etching with buffered oxide etchant (BOE). The SiO₂ DI is not etched by BOE since it is covered by an Ag NP. After a thermal annealing process at 300 °C for 30 min with ambient nitrogen, REG Ag NPs of smooth surface can be obtained. Figure 1a schematically demonstrates the device structure around an Ag NP with a SiO₂ DI. Figure 2a shows a tilted scanning electron microscopy (SEM) image of the REG Ag NPs in sample C1, i.e., with a SiO₂ DI of ~ 3 nm in thickness. Figure 2b shows the cross-sectional transmission electron microscopy (TEM) image of sample C1 around an Ag NP. Here, the bright stripe beneath the dark Ag NP region corresponds to the ~ 3 -nm SiO₂ DI. In the case of a GaZnO DI, a GaZnO layer of ~ 10 nm is deposited onto p-GaN before the formation of the patterned mask. After the complete procedure of REG Ag NP fabrication, the whole GaZnO layer is preserved, as schematically shown in Fig. 1b. GaZnO is a good transparent conductor under direct-current operation, but is a dielectric material in the optical spectral range with the refractive index around 1.8. The GaZnO layer is deposited with molecular beam epitaxy at

Table 1 Sample parameters of samples A1-E1, A1'-E1', A5-E5, and A5'-E5'

Sample	QW no.	p-GaN thick. (nm)	NP size (nm)	DI condition	Trans. min. wavelength (nm)	Trans. min. level (%)	Trans. level at 470 nm (%)	Dip FWHM (nm)
A1/A5 (A1'/A5')	1/5	50 (120)	–	–	–	–	–	–
B1/B5 (B1'/B5')	1/5	50 (120)	85.3	No DI	512–512	27.0–27.7	65.8–66.1	84–86
C1/C5 (C1'/C5')	1/5	50 (120)	52.2	Thin SiO ₂	494–497	41.9–42.9	47.4–48.2	135–136
D1/D5 (D1'/D5')	1/5	50 (120)	47.2	Thick SiO ₂	482–487	47.4–48.5	49.9–50.5	154–156
E1/E5 (E1'/E5')	1/5	50 (120)	76.4	GaZnO	502–506	36.5–37.0	50.1–50.8	117–118

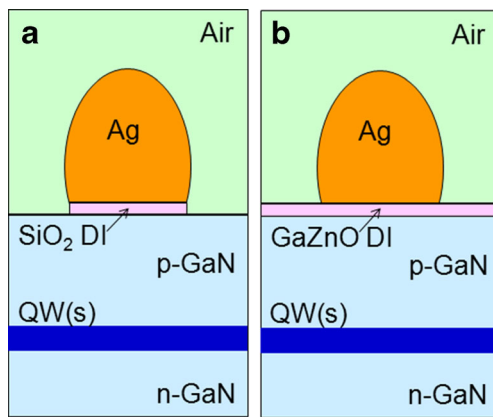


Fig. 1 **a** Schematic demonstration of the device structure around a surface Ag NP when a SiO₂ DI is used. **b** Schematic demonstration of the device structure around a surface Ag NP when a GaZnO DI is used

350 °C in substrate temperature. Its resistivity, mobility, and electron concentration are $1.6 \times 10^{-4} \Omega\text{-cm}$, $22 \text{ cm}^2/\text{V-s}$, and $1.5 \times 10^{21} \text{ cm}^{-3}$, respectively [30]. Also, the transmission of a GaZnO layer of 250 nm in thickness is higher than 90 % in the visible range. In all samples described above, a Ni (5 nm)/Au (5 nm) current spreading layer is added to the sample top surfaces.

RAN Ag NPs are also fabricated on the epitaxial structures of thin p-GaN (including single- and multiple-QW structures) for comparing their LED performances with those of REG Ag NPs. Based on the epitaxial structure of thin p-GaN and single-QW, samples B1R-E1R are processed with RAN surface Ag NPs but without DI (B1R), with RAN surface Ag NPs and a SiO₂ layer of 3 nm in thickness as the DI (C1R), with RAN surface Ag NPs and a SiO₂ layer of 6 nm in thickness as the DI (D1R), and with RAN surface Ag NPs and a GaZnO layer of 10 nm in thickness as the DI (E1R), respectively. In this sample series, sample A1 assigned earlier can also be used as the reference sample. The same Ag NP and DI conditions are implemented on the epitaxial structure of

thin p-GaN and multiple-QW for fabricating samples B5R-E5R. In this sample series, sample A5 assigned earlier can also be used as the reference sample. The detailed descriptions of samples B1R-E1R and B5R-E5R, including the average Ag NP sizes, are given in columns 2–5 of Table 2. The RAN Ag NPs are formed by depositing an Ag layer of 2 nm in thickness on either p-GaN or various DIs, followed by a thermal annealing process for 30 min at 300 °C with ambient nitrogen. Under different surface conditions, the formed Ag NPs have different sizes. It is noted that the portions of the SiO₂ DI layers in samples C1R, D1R, C5R, and D5R not covered by Ag NPs are removed through a dry etching process to expose p-GaN for depositing a thin Ni/Au current spreading layer. However, the whole GaZnO DI layers in samples E1R and E5R are preserved on the device beneath the thin Ni/Au current spreading layer. Figure 3a shows a tilted SEM image of the RAN Ag NPs on sample C1R. Figure 3b shows a cross-sectional TEM image of a few Ag NPs in sample C1R. Here, the bright stripes below the dark Ag regions correspond to the SiO₂ DI. LEDs of the standard configuration with a mesa dimension of $300 \mu\text{m} \times 300 \mu\text{m}$ are processed for all the assigned 28 samples.

Figure 4 shows the transmission spectra of samples B1-E1, B1'-E1', B5-E5, and B5'-E5', which are normalized by those of individual reference samples (A1, A1', A5, and A5'), after Fabry-Perot oscillations are filtered. Here, one can see that all the transmission curves of the same DI condition are very close, indicating the stability of Ag NP fabrication. In Fig. 4, a depression corresponds to the extinction caused by the mixed feature of the dipole and higher order LSP resonance modes of the Ag NPs. One can see that by adding a DI, the depression minimum is blue shifted and its depth is reduced, implying that the major LSP resonance wavelength becomes shorter and the resonance strength becomes weaker after a DI is applied. Columns 6 and 7 of Table 1 show the ranges of the transmission minimum wavelength and the corresponding

Fig. 2 **a** Tilted SEM image of the REG Ag NPs in sample C1. **b** Cross-sectional TEM image of sample C1 around a surface Ag NP

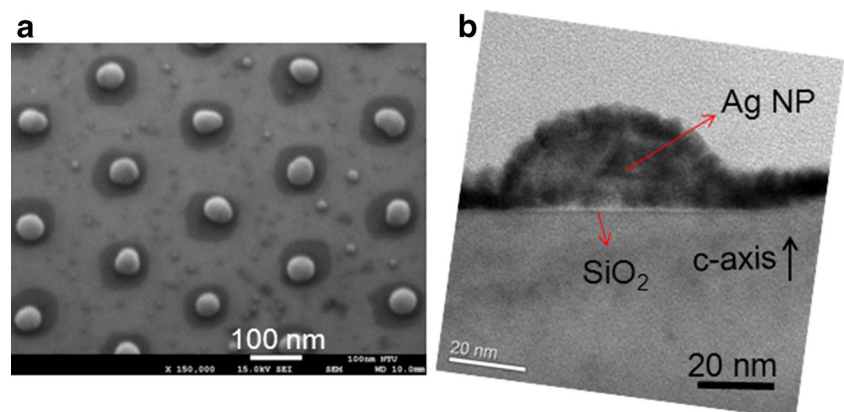


Table 2 Sample parameters of samples B1R-E1R and B5R-E5R

Sample	QW no.	p-GaN thick. (nm)	NP size (nm)	DI condition	Trans. min. wavelength (nm)	Trans. min. level (%)	Trans. level at 470 nm (%)	Dip FWHM (nm)
B1R/B5R	1/5	50	58.4	No DI	514–515	39.9–40.1	59.4–59.6	119–119
C1R/C5R	1/5	50	35.5	Thin SiO ₂	476–476	48.8–49.3	49.5–50.0	143–143
D1R/D5R	1/5	50	24.2	Thick SiO ₂	462–463	51.2–51.8	51.9–52.0	162–163
E1R/E5R	1/5	50	43.2	GaZnO	478–480	46.3–46.3	47.1–47.5	129–130

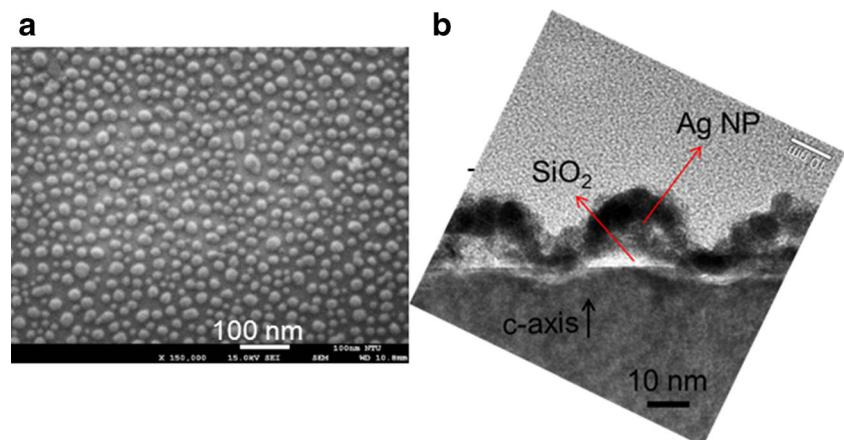
minimum level in various samples. Those ranges are quite narrow. The QW emission wavelength at 470 nm is indicated by a vertical dashed line in Fig. 4. In column 8 of Table 1, we show the ranges of the transmission level at 470 nm. Here, one can see that the blue-shift range of the transmission minimum increases with increasing DI thickness and decreases with increasing DI refractive index. The lowest transmission level at 470 nm among those samples with DIs can be seen in the sample group of C1, C1', C5, and C5'. A lower transmission level at the QW emission wavelength implies a stronger LSP resonance at this wavelength and can result in a stronger SP coupling effect. Figure 5 shows the transmission spectra of samples B1R-E1R and B5R-E5R, which are normalized by those of individual reference samples (A1 and A5), after Fabry-Perot oscillations are filtered. The variation trend in Fig. 5 is the same as that in Fig. 4. Columns 6 and 7 of Table 2 show the ranges of the transmission minimum wavelength and the corresponding minimum level of samples B1R-E1R and B5R-E5R. Again, those ranges are quite narrow. The QW emission wavelength at 470 nm is also indicated by a vertical dashed line in Fig. 5. In column 8 of Table 2, we show the ranges of the transmission level at 470 nm. Here, the lowest transmission level at 470 nm among samples B1R-E1R (B5R-E5R) is observed in sample E1R (E5R). By comparing Fig. 4 with Fig. 5, one can see that the depressions induced by REG Ag NPs (Fig. 4) are generally narrower

than those induced by RAN Ag NPs (Fig. 5). The ranges of the full-width at half-maximum (FWHM) of the depressions in Figs. 4 and 5 are listed in the rightmost columns of Tables 1 and 2, respectively. Here, one can see that the depression FWHM under each DI condition of REG Ag NPs is smaller than that of RAN Ag NPs. This result can be attributed to the more non-uniform NP size distribution in the RAN NPs.

Photoluminescence Characterization Results

IQEs of the fabricated samples are evaluated based on PL measurement excited by an InGaN laser diode at 406 nm with 5 mW in power. The ratio of the integrated PL intensity at 300 K over that at 10 K is usually regarded as the IQE of a sample. The IQEs of samples A1-E1 and A1'-E1' are listed in row 2 of Table 3 (the numbers before slashes). Those of samples A5-E5 and A5'-E5' are listed in row 2 of Table 4 (the numbers before slashes). The numbers after slashes in rows 2 of Tables 3 and 4 represent the ratios with respect to the individual reference samples (samples A1, A1', A5, and A5'). In Table 3, one can see that the intrinsic IQE of the epitaxial structure of thick p-GaN (32.1 % in sample A1') is higher than that of the epitaxial structure of thin p-GaN (21.9 % in sample A1). The growth of a thicker p-GaN layer can lead to a thermal annealing process of the QW and hence improve the QW quality [21]. By fabricating Ag NPs on the surface, the IQE

Fig. 3 **a** Tilted SEM image of the RAN Ag NPs in sample C1R. **b** Cross-sectional TEM image of sample C1R around a surface Ag NP



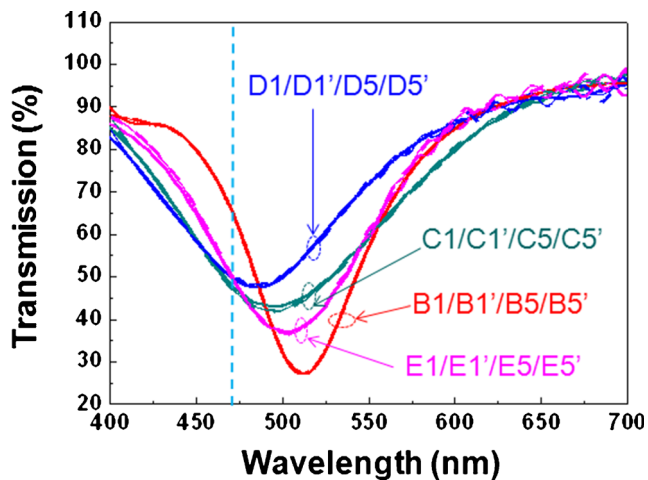


Fig. 4 Normalized transmission spectra of samples B1-E1, B1'-E1', B5-E5, and B5'-E5' after Fabry-Perot oscillations are filtered. The vertical dashed line indicates the emission wavelength of the QWs

is enhanced in either sample group of A1-E1 or A1'-E1'. Among samples B1-E1, the insertions of the DIs lead to higher IQEs. In particular, an increase by 92 % is obtained in sample C1. The variation trend of the IQE among samples B1-E1 is consistent with that of the transmission level at 470 nm, as shown in Fig. 3 and Table 1. A lower transmission level at 470 nm corresponds to a stronger SP coupling effect and hence a higher IQE. Among samples B1'-E1', the insertions of the DIs slightly increase their IQEs. The intrinsic IQEs of the epitaxial structures with five QWs (25.6 and 38.5 % in samples A5 and A5', respectively) are higher than those of the corresponding samples with single QW (21.9 and 32.1 % in samples A1 and A1', respectively), indicating that the QW quality of a multiple-QW structure can be superior to that of a single-QW structure. Among samples A5-E5, the variation trend of IQE is the same as that among samples A1-E1. However, the IQE enhancement ratios of samples B5-E5 are lower

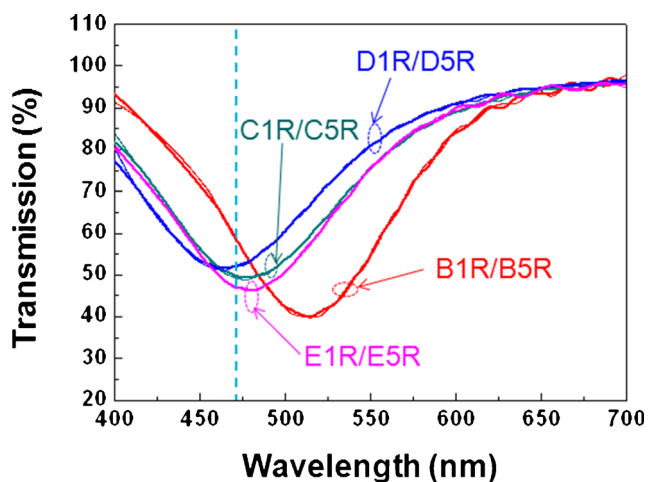


Fig. 5 Normalized transmission spectra of samples B1R-E1R and B5R-E5R after Fabry-Perot oscillations are filtered. The vertical dashed line indicates the emission wavelength of the QWs

than the corresponding values of samples B1-E1. Among samples A5'-E5', again the addition of either Ag NPs or DI to the device results in a slight increase of IQE.

Figure 6 shows the normalized time-resolved PL (TRPL) profiles of samples A1-E1 and A1'-E1'. The TRPL is measured with the excitation of the second-harmonic (390 nm) of a fs Ti:sapphire laser (5 mW in average power). The exponentially fitted decay times of those TRPL profiles are listed in row 3 of Table 3. Here, one can see that the variation trend of PL decay time among samples A1-E1 is consistent with that of IQE, confirming the significant SP coupling effects in samples B1-E1. A stronger SP coupling effect leads to a higher emission rate and hence a higher decay rate of carrier density. The similar TRPL profiles of samples A5-E5 and A5'-E5' are obtained for fitting to give the PL decay times in row 3 of Table 4. The variation trend of the PL decay time among samples A5-E5 is the same as that among samples A1-E1 and is consistent with the corresponding variation trend of IQE. It is noted that the larger IQE of sample A1' (A5'), when compared with that of sample A1 (A5), originates from its relatively lower non-radiative recombination rate such that its PL decay time is longer. However, with Ag NPs in samples B1-E1 and B1'-E1' (samples B5-E5 and B5'-E5'), the emission rates are enhanced such that the IQEs are increased and the PL decay times are reduced.

Performances of the LEDs with Regularly Patterned Ag Nanoparticles

Figure 7 shows the variations of the normalized output intensities of samples A1-E1 and A1'-E1' with injection current (I - I curves). The LED output intensity of a sample is obtained by summing those from the top and bottom sides. The relative output intensities with respect to those of individual reference samples (samples A1 and A1') when injection currents are 5 and 100 mA are listed in rows 4 and 5 of Table 3, respectively. Here, one can see that in all the samples, the output intensity enhancements at 5 mA in injection current are about the same as the corresponding values at 100 mA. The numbers after the slashes in row 5 show the relative output intensities of all the ten samples with respect to that of sample A1 when injection current is 100 mA. In Table 3, we can see that the variation trend of the output intensity among samples A1-E1 is consistent with that of IQE. Also, similar to the variation of IQE, the output intensity enhancement by adding surface Ag NPs or DI is smaller in samples A1'-E1', when compared with samples A1-E1. The larger enhancement ratios in samples B1-E1 indicate that the SP coupling strengths in samples B1-E1 are significantly stronger because of their shorter distance between the Ag NPs and the QW. However, it is noted that even with a significantly larger enhancement ratio through SP coupling in sample B1, its output intensity is still lower than those

Table 3 Characterization results of samples A1-E1 and A1'-E1'

Sample	A1	B1	C1	D1	E1	A1'	B1'	C1'	D1'	E1'
IQE (%)	21.9/1	31.2/1.42	42.0/1.92	38.8/1.77	34.6/1.58	32.1/1	33.6/1.05	34.4/1.07	34.3/1.07	33.9/1.06
PL decay time (ns)/decay rate ratio	3.15/1	2.42/1.30	1.19/2.65	1.87/1.68	2.19/1.44	3.62/1	2.99/1.21	2.67/1.36	2.61/1.39	2.93/1.24
Relative intensity at 5 mA	1	1.35	1.75	1.65	1.47	1	1.12	1.19	1.23	1.16
Relative intensity at 100 mA	1/1	1.36/1.36	1.77/1.77	1.66/1.66	1.47/1.47	1/1.22	1.13/1.40	1.21/1.48	1.24/1.51	1.16/1.42
Device resistance (Ω)	25.7	26.9	29	29.9	27.8	24.5	25.4	28.6	29.3	27.1
EQE droop range (%)	58.3	40.2	26.3	30.6	32.7	46.8	43.9	40.6	38.5	42.7
-3 dB frequency (MHz)/ratio	8.6/1	12.2/1.42	13.5/1.57	13.1/1.52	12.6/1.47	8.3/1	8.8/1.06	10.2/1.23	10.9/1.31	9.3/1.12

of samples B1'-E1' since the epitaxial structure of sample A1'-E1' has a higher intrinsic IQE. The corresponding relative intensities of samples A5-E5 and A5'-E5' with respect to those of individual reference samples (samples A5 and A5') when injection currents 5 and 100 mA are listed in rows 4 and 5 of Table 4, respectively. The variation trends of the relative output intensity in samples A5-E5 and A5'-E5' are all the same as those of samples A1-E1 and A1'-E1'. However, the enhancement ratios in samples A5-E5 and A5'-E5' are slightly lower. The largest enhancement ratio is only 69 % in sample C5, which is smaller than that of 77 % in sample C1.

As shown in Tables 3 and 4, with the SiO₂ DIs (samples C1, D1, C5, and D5), the IQE and output intensity are further enhanced, when compared with samples B1 and B5. A thinner SiO₂ DI (samples C1 and C5) leads to a larger enhancement. With a GaZnO layer as the DI, the SP coupling effect becomes weaker and hence the IQE and output intensity become smaller. This variation trend is consistent with that of the transmission level at 470 nm, as shown in column 8 of Table 1. A lower transmission level corresponds to a stronger LSP resonance at this wavelength and hence a stronger SP coupling effect for generating a larger IQE and stronger output intensity. Among samples B1'-E1' and B5'-E5', the variation trends of output intensity are different from those of samples B1-E1 and B5-E5, and hence are different from that of the transmission level at 470 nm. Such differences indicate that the output intensity increases in samples B1'-E1'

and B5'-E5' have other causes besides a weak SP coupling effect. The weak SP coupling leads to the slight increases of IQE. The variation trend of IQE among samples B1'-E1' or B5'-E5' is the same as that among samples B1-E1 or B5-E5. The increases of output intensity in samples B1'-E1' or B5'-E5', which have larger increase ratios than IQE, are attributed to the light extraction enhancement besides the weak SP coupling effect. The light extraction enhancement is caused by the non-resonant scattering and absorption-reemission process of the Ag NPs, and the graded refractive index structure after a DI is added. In particular, with a thicker DI of a lower refractive index in samples D1' or D5', the light extraction efficiency is more significantly increased.

Figure 8 shows the relations between injection current and applied voltage (*I-V* curves) of samples A1-E1 and A1'-E1'. The insert shows the magnified portion between 5.6 and 6.5 V to clearly differentiate those *I-V* curves. The resistance levels of those devices are listed in row 6 of Table 3. Here, one can see that the resistance levels of samples A1-E1 are slightly larger than those of the corresponding samples in group A1'-E1', indicating that a thicker p-GaN layer leads to a better electrical property in the LED device. In the same group of sample, the fabrication of surface Ag NPs or the addition of a DI results in higher device resistance. In particular, a SiO₂ DI leads to higher resistance, when compared with the case of a GaZnO DI. The sample with a thicker SiO₂ DI

Table 4 Characterization results of samples A5-E5 and A5'-E5'

Sample	A5	B5	C5	D5	E5	A5'	B5'	C5'	D5'	E5'
IQE (%)	25.6/1	34.8/1.36	44.8/1.75	42.5/1.66	37.6/1.47	38.5/1	39.2/1.02	40.8/1.06	40.5/1.05	39.6/1.03
PL decay time (ns)/decay rate ratio	3.16/1	2.42/1.31	1.23/2.57	1.91/1.65	2.22/1.42	3.63/1	3.04/1.19	2.67/1.36	2.64/1.38	2.97/1.22
Relative intensity at 5 mA	1	1.32	1.68	1.61	1.39	1	1.12	1.18	1.21	1.14
Relative intensity at 100 mA	1/1	1.33/1.33	1.69/1.69	1.61/1.61	1.41/1.41	1/1.20	1.12/1.35	1.19/1.43	1.22/1.47	1.14/1.37
Device resistance (Ω)	25.2	26.3	29.2	30.2	27.7	24.2	24.7	28.4	28.7	26.2
EQE droop range (%)	54.5	42.8	29.0	33.9	37.2	43.2	41.0	37.8	35.7	39.8
-3 dB frequency (MHz)/ratio	8.4/1	12.1/1.44	13.4/1.60	12.9/1.54	12.5/1.49	8.2/1	8.7/1.06	10.0/1.22	10.5/1.28	9.1/1.11

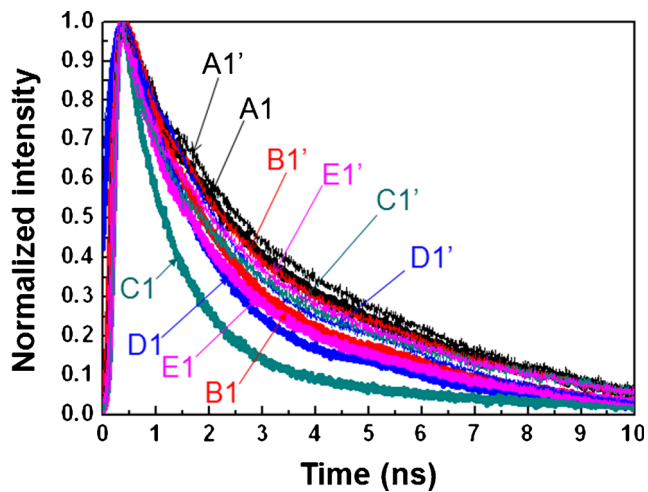


Fig. 6 Normalized TRPL profiles of samples A1-E1 and A1'-E1'

(D1 or D1') has a higher resistance level, when compared to that with a thinner SiO₂ DI (C1 or C1'). The device resistance levels of samples A5-E5 and A5'-E5' are listed in row 6 of Table 4. Their values are about the same as those of the corresponding samples of A1-E1 and A1'-E1'. Also, the variation trends are identical.

Figure 9 shows the relative external quantum efficiencies (EQEs), normalized to the maximum level of sample B1, as functions of injection current of samples A1-E1 and A1'-E1'. When injection current is larger than 20 mA, all the samples show the efficiency droop behaviors. However, those samples with surface Ag NPs show the higher maximum EQEs and weaker droop effects, when compared with the individual reference samples (samples A1 and A1'). In each sample group, the variation trends of the maximum EQE and droop effect are the same as that of LED output intensity. The droop range, which is defined as the percentage difference between the

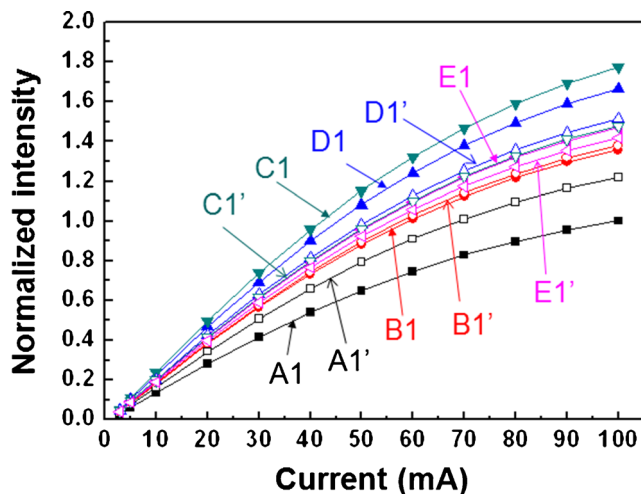


Fig. 7 Variations of the normalized output intensities of samples A1-E1 and A1'-E1' with injection current

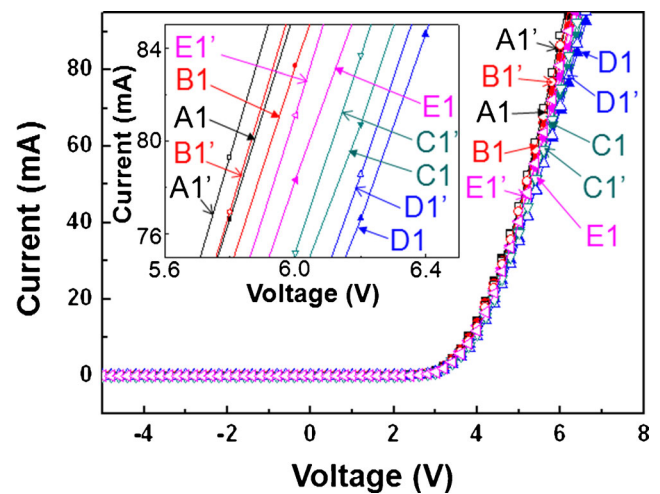


Fig. 8 Relations between injection current and applied voltage of samples A1-E1 and A1'-E1'. The *insert* shows the magnified portion between 5.6 and 6.5 V to clearly differentiate those curves

relative EQE at 100 mA in injection current and the individual maximum level of relative EQE, of each sample is shown in row 7 of Table 3. Here, we can see that the variation trend of the droop range among the samples in the same group is consistent with that of LED output intensity. It is interesting to note that although the LED output intensities of samples B1', C1', and E1' are higher than that of sample B1, their droop ranges are also larger than that of sample B1, indicating that the significant SP coupling effect in sample B1 can indeed effectively reduce the droop effect. The droop ranges of samples A5-E5 and A5'-E5' are shown in row 7 of Table 4. Their variation trends are the same as those of samples A1-E1 and A1'-E1'.

Figure 10 shows the modulation responses as functions of modulation frequency for samples A1-E1 and A1'-E1'.

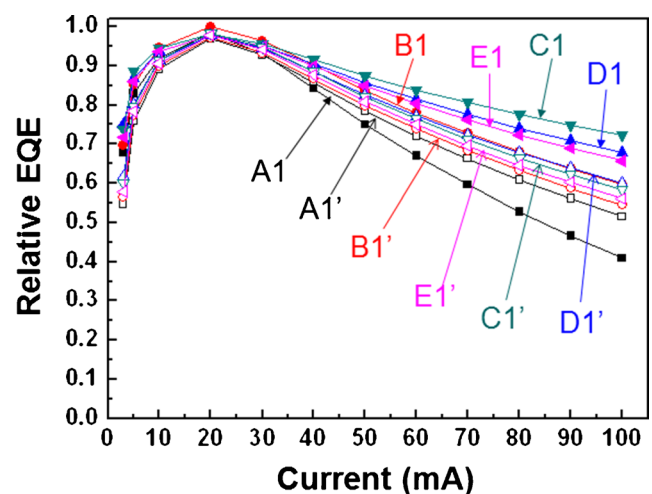


Fig. 9 Relative EQEs, normalized to the maximum level of sample B1, as functions of injection current of samples A1-E1 and A1'-E1'

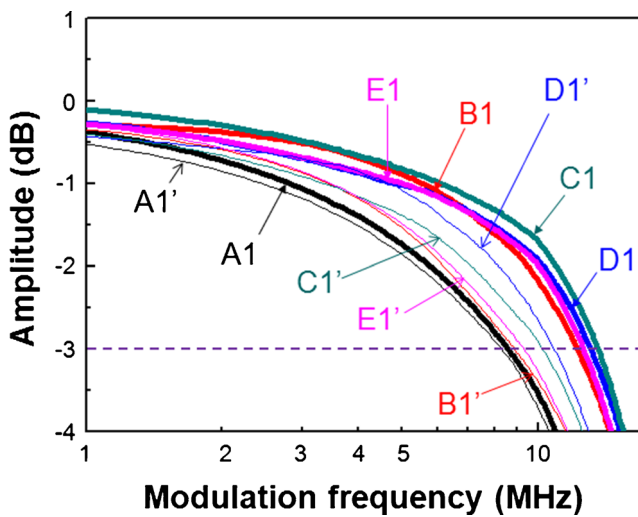


Fig. 10 Modulation responses as functions of modulation frequency for samples A1-E1 and A1'-E1'. The signal amplitude is normalized to the level at zero modulation frequency

The signal amplitude is normalized to the level at zero modulation frequency. Therefore, all the curves in Fig. 10 converge to 0 dB under the condition of direct-current (DC) drive. Normally, in such a modulation response profile, the modulation frequency for the amplitude to drop 3 dB from the DC level is defined as the -3-dB frequency, as indicated by the horizontal dashed line in Fig. 10. Here, one can see that the -3-dB frequencies of all the samples with Ag NPs or DIs are higher than those of the reference samples (A1 and A1'). In particular, those four samples with effective SP coupling (samples B1-E1) are significantly increased. The modulation -3-dB frequencies of all the ten samples are listed in the bottom row of Table 3. It is increased from 8.6 MHz in sample A1 to 13.5 MHz in sample C1 among samples A1-E1. Among samples A1'-E1', the -3-dB frequency is increased from 8.3 MHz in sample A1' to 10.9 MHz in sample D1'. The variation trend of the -3-dB frequency among all those samples is consistent with those of the

output intensity and IQE. The modulation -3-dB frequencies of samples A5-E5 and A5'-E5' are listed in the bottom row of Table 4. They are close to the corresponding values of samples A1-E1 and A1'-E1' and follow the same variation trend.

Performances of the LEDs with Randomly Distributed Ag Nanoparticles

Although the LSP resonance peak wavelengths of RAN and REG Ag NPs are different, the variation behaviors after adding the DIs of the two LED sample groups are similar, as shown in Fig. 5, except that the lowest transmission level at the QW emission peak (470 nm) is observed in the samples with the GaZnO DI (samples E1R and E5R), instead of those with the thin SiO₂ DI (samples C1, C5, C1', and C5'). The characterization results of the LED samples with RAN Ag NPs (samples B1R-E1R and B5R-E5R) are shown in Table 5. For comparison, the results of the reference samples A1 and A5 are also shown in this table. With the lowest transmission levels at 470 nm in samples E1R and E5R, their PL decay times are the shortest, their IQEs and output intensities are the highest, their EQE droop ranges are the smallest, and their modulation -3-dB frequencies are the highest among the individual sample groups of the same QW number. The enhancement ratios of IQE and output intensity in sample E1R, with respect to its reference sample A1, can reach 97 and 87 %, respectively, which are higher than the corresponding values in sample C1 (92 and 77 %, respectively). Also, the enhancement ratios of IQE and output intensity in sample E5R, with respect to its reference sample A5, can reach 83 and 78 %, respectively, which are higher than the corresponding values in sample C5 (75 and 69 %, respectively). The PL decay times of samples E1R and E5R are 0.83 and 0.94 ns, which are shorter than the corresponding values of 1.19 and 1.23 ns of samples C1 and C5, respectively. Meanwhile, the EQE droop ranges of samples E1R and E5R are 21.4 and 23.5 %, which are smaller than the corresponding values of

Table 5 Characterization results of samples B1R-E1R and B5R-E5R. For comparison, the results of samples A1 and A5 are repeated here

Sample	A1	B1R	C1R	D1R	E1R	A5	B5R	C5R	D5R	E5R
IQE (%)	21.9/1	32.2/1.47	40.0/1.83	37.2/1.70	43.2/1.97	25.6/1	36.2/1.41	43.8/1.71	41.5/1.62	46.8/1.83
PL decay time (ns)/decay rate ratio	3.15/1	2.25/1.40	1.59/1.98	1.93/1.63	0.83/3.80	3.16/1	2.31/1.37	1.65/1.92	2.16/1.46	0.94/3.36
Relative intensity at 5 mA	1	1.39	1.72	1.64	1.86	1	1.38	1.66	1.58	1.76
Relative intensity at 100 mA	1	1.41	1.73	1.64	1.87	1	1.39	1.66	1.59	1.78
Device resistance (Ω)	25.7	27.4	30.4	33.2	28.5	25.2	26.8	31.7	32.2	28.1
EQE droop range (%)	58.3	37.8	23.2	28.2	21.4	54.5	39.9	26.8	31.4	23.5
-3 dB frequency (MHz)/ratio	8.6/1	12.3/1.43	13.3/1.55	12.8/1.49	13.7/1.59	8.4/1	12.3/1.46	13.2/1.57	12.7/1.51	13.7/1.63

26.3 and 29.0 % of samples C1 and C5, respectively. In addition, the modulation -3 -dB frequencies of samples E1R and E5R are the same at 13.7 MHz, which is larger than the corresponding values of 13.5 and 13.4 MHz of samples C1 and C5, respectively. Those comparisons indicate that the SP coupling effects in samples E1R and E5R are stronger than those of the corresponding samples of C1 and C5, respectively. However, if we compare the device resistance between samples C1R/C5R and C1/C5, the samples with REG Ag NPs (samples C1/C5) have superior performances. The variation trend of device resistance among samples B1R-E1R (B5R-E5R) is the same as that among samples B1-E1 (B5-E5). The addition of Ag NPs or DI results in higher device resistance. Among the samples with DIs, the use of GaZnO as the DI always leads to lower resistance.

Discussions

As mentioned in “Performances of the LEDs with Regularly Patterned Ag Nanoparticles” section, the performances of the LED samples with thin p-GaN are strongly influenced by the LSP coupling effect, which depends on the conditions of Ag NP and DI. On the other hand, the behaviors of the LED samples with thick p-GaN are related to the Ag NP-induced light extraction enhancement and a weak LSP coupling effect. It is usually believed that SP coupling can also enhance the light extraction efficiency of an LED. The light extraction efficiency can indeed be enhanced through the angle redistribution of emitted photon in the SP coupling process [21]. However, in the current situation of thick p-GaN, the SP coupling effect is weak, as can be seen in the increase of IQE by only a few percent (see Tables 3 and 4). Therefore, the enhancement of light extraction is expected to be mainly caused by the non-resonant scattering of surface Ag NPs, the SP-induced absorption-reemission process, and the graded refractive index structure after a DI is added. The SP-induced absorption-reemission process means that the emitted photons from the QWs are absorbed by Ag NPs and part of them is reemitted through SP resonance. The SP-induced absorption-reemission process is different from the SP coupling mechanism. In the SP coupling mechanism, energy is directly transferred into an SP mode for emission without going through the form of photon. The other issue deserving mentioning in the LEDs of thick p-GaN is that because it has a higher intrinsic IQE, when compared with that of thin p-GaN, the IQE enhancement through SP coupling is less effective. A QW with a higher IQE leads to a less effective SP coupling process in terms of emission efficiency enhancement [6, 31].

By comparing the results between the single-QW and multiple-QW samples with significant SP coupling (thin p-GaN), i.e., between samples A1-E1 and A5-E5 and between samples A1R-E1R and A5R-E5R, first we can see that the

intrinsic IQE of the five-QW epitaxial structure (25.6 %) is higher than that of the single-QW epitaxial structure (21.9 %). As mentioned earlier, an LED with a QW structure of a higher IQE usually leads to a weaker SP coupling effect, i.e., a smaller output intensity enhancement ratio [6, 31]. From Tables 3, 4, and 5, either with REG or with RAN Ag NPs, one can see that by adding Ag NPs or DIs, the samples of single-QW indeed have higher IQE and output intensity enhancement ratios, shorter PL decay times, smaller EQE droop ranges, and slightly larger modulation -3 dB frequencies, when compared with the corresponding samples of five-QW. Such a behavior can also be related to the depth distribution of QW in a multiple-QW sample. With 3 and 10 nm for the well and barrier thicknesses, respectively, the distances between the first through fifth QW (counted from the top) and the bottom of Ag NPs are 80, 93, 106, 119, and 132 nm, respectively, before a DI is added. The SP coupling effect of a QW diminishes with distance. In this situation, the overall emission enhancement of a multiple-QW sample is expected to be smaller, when compared with the corresponding single-QW sample because not all the QWs have the same SP coupling strength as the top one. However, theoretically an SP mode can couple with all the nearby radiating dipoles. It is possible that an SP mode can simultaneously couple with the dipoles in two neighboring QWs for coherent emission. Nevertheless, this issue requires further investigation.

Between the samples with REG and RAN Ag NPs, although the variation trends of the SP coupling effect are essentially the same, a few differences deserve discussions. (1) Because of the more uniform geometry distribution among REG Ag NPs, their depression features in transmission spectra are deeper and narrower, when compared with those of RAN Ag NPs, as shown in Figs. 4 and 5. Such a difference in extinction feature can affect the LSP resonance strength and hence the coupling strength at the QW emission wavelength. (2) The LSP resonance behavior is also affected by the NP size. As shown in Tables 1 and 2, either with the REG or RAN Ag NPs, the NP size varies with the DI condition. The NP size variation is related to the adhesion of Ag onto the substrate with a DI. From the results of Ag NP size, we speculate that the adhesion of Ag onto SiO₂ is the weakest among the three surface materials (GaN, SiO₂, and GaZnO). With weak adhesion, surface tension can lead to a more sphere-like NP and hence a smaller planar NP size during the thermal annealing process. Between the REG and RAN Ag NPs, because the fabricated hole diameter for forming REG Ag NPs is as large as 100 nm through nano-imprint, the REG Ag NP sizes are generally larger than those of RAN Ag NPs. (3) In practical application, the fabrication of RAN Ag NPs is much simpler and hence is significantly cheaper, when compared with the fabrication of REG Ag NPs.

From rows 3 and 8 of Tables 3, 4, and 5, we can see that the ratios of PL decay rate (with respect to individual reference

samples) can be quite different from those of modulation -3 dB frequency, particularly for those samples of strong SP coupling, including samples C1, C5, E1R, and E5R. In these samples, the PL decay times are significantly reduced and hence their decay rate ratios are larger than two. However, the increase ratios of the corresponding modulation -3 dB-frequencies are significantly smaller. For instance, in sample C1, the PL decay rate is increased by 165 %; however, the modulation -3 -dB frequency is increased only by 57 %. Such results indicate that the modulation response of an LED is mainly controlled by the RC time constant of the device, instead of the carrier decay rate in the QWs. Although the enhancement of carrier decay rate through SP coupling can increase the modulation -3 -dB frequency, the increase is limited to several tens percent. The device RC time constant can be significantly reduced by decreasing the mesa size of the device [26, 27]. The dependence of the increase range of the modulation -3 -dB frequency due to SP coupling on device mesa size is an issue deserving further investigation. If an increase range of several tens percent in modulation -3 dB frequency can always be achieved through SP coupling when the LED mesa size is reduced, the SP coupling contribution to modulation response of an LED will be important.

Conclusions

In summary, we have first demonstrated the enhanced SP coupling effects in a blue LED with REG surface Ag NPs on a DI of a lower refractive index overgrown on p-GaN. Without a DI, the surface Ag NPs-induced SP coupling with the QWs in the LED could lead to the increases of IQE and LED output intensity, the reduction of the EQE droop effect, and the enhancement of modulation response. By adding a DI, the SP coupling effect was enhanced, resulting in the further improvements of all the aforementioned factors. The SP coupling effects in the LEDs with REG Ag NPs on DIs were compared to those of RAN Ag NPs previously reported. Although the variation trends of LSP resonance peaks and hence SP coupling behaviors of REG and RAN Ag NPs were similar, their LSP resonance strengths at the QW emission wavelength were quite different due to their different spectral patterns of LSP resonance. In other words, although the REG Ag NPs could produce stronger collective LSP resonance with a narrower spectral width, the SP coupling effect depended mainly on the LSP resonance strength at the QW emission wavelength. The SP coupling effects in the LED samples with single-QW were also compared with those of multiple-QW.

Acknowledgments This research was supported by Ministry of Science and Technology, Taiwan, The Republic of China, under the grants of NSC 102-2221-E-002-204-MY3, 102-2120-M-002-006, and 102-2221-E-002-199, by the Excellent Research Projects of National Taiwan

University (103R890951 and 103R890952), and by US Air Force Scientific Research Office under the contract of AOARD-13-4143.

References

1. Yeh DM, Huang CF, Chen CY, Lu YC, Yang CC (2007) Surface plasmon coupling effect in an InGaN/GaN single-quantum-well light-emitting diode. *Appl Phys Lett* 91(17):171103
2. Sun G, Khurgin JB, Soref RA (2007) Practicable enhancement of spontaneous emission using surface plasmons. *Appl Phys Lett* 90(11):111107
3. Shen KC, Chen CY, Chen HL, Huang CF, Kiang YW, Yang CC, Yang YJ (2008) Enhanced and partially polarized output of a light-emitting diode with its InGaN/GaN quantum well coupled with surface plasmons on a metal grating. *Appl Phys Lett* 93(23):231111
4. Kwon MK, Kim JY, Kim BH, Park IK, Cho CY, Byeon CC, Park SJ (2008) Surface-plasmon-enhanced light-emitting diodes. *Adv Mater* 20(7):1253–1257
5. Lin J, Mohammadzija A, Neogi A, Morkoç H, Ohtsu M (2010) Surface plasmon enhanced UV emission in AlGaIn/GaN quantum well. *Appl Phys Lett* 97(22):221104
6. Kuo Y, Ting SY, Liao CH, Huang JJ, Chen CY, Hsieh C, Lu YC, Chen CY, Shen KC, Lu CF, Yeh DM, Wang JY, Chuang WH, Kiang YW, Yang CC (2011) Surface plasmon coupling with radiating dipole for enhancing the emission efficiency of a light-emitting diode. *Opt Express* 19(S4):A914–A929
7. Cho CY, Lee SJ, Song JH, Hong SH, Lee SM, Cho YH, Park SJ (2011) Enhanced optical output power of green light-emitting diodes by surface plasmon of gold nanoparticles. *Appl Phys Lett* 98(5):051106
8. N. Gao, K. Huang, J. Li, S. Li, X. Yang, and J. Kang (2012) Surface-plasmon-enhanced deep-UV light emitting diodes based on AlGaIn multi-quantum wells, *Scientific Reports* 2(#816), 00816
9. Chen HS, Chen CF, Kuo Y, Chou WH, Shen CH, Jung YL, Kiang YW, Yang CC (2013) Surface plasmon coupled light-emitting diode with metal protrusions into p-GaN. *Appl Phys Lett* 102(4):041108
10. Cho CY, Zhang Y, Cicek E, Rahnema B, Bai Y, McClintock R, Razeghi M (2013) Surface plasmon enhanced light emission from AlGaIn-based ultraviolet light-emitting diodes grown on Si (111). *Appl Phys Lett* 102(21):211110
11. Schubert MF, Xu J, Kim JK, Schubert EF, Kim MH, Yoon S, Lee SM, Sone C, Sakong T, Park Y (2008) Polarization-matched GaInN/AlGaInN multi-quantum-well light-emitting diodes with reduced efficiency droop. *Appl Phys Lett* 93(4):041102
12. Xie J, Ni X, Fan Q, Shimada R, Özgür Ü, Morkoç H (2008) On the efficiency droop in InGaIn multiple quantum well blue light emitting diodes and its reduction with p-doped quantum well barriers. *Appl Phys Lett* 93(12):121107
13. Maier M, Köhler K, Kunzer M, Pletschen W, Wagner J (2009) Reduced nonthermal rollover of wide-well GaInN light-emitting diodes. *Appl Phys Lett* 94(4):041103
14. Delaney KT, Rinke P, Van de Walle CG (2009) Auger recombination rates in nitrides from first principles. *Appl Phys Lett* 94(19):191109
15. Kioupakis E, Rinke P, Delaney KT, Van de Walle CG (2011) Indirect Auger recombination as a cause of efficiency droop in nitride light-emitting diodes. *Appl Phys Lett* 98(16):161107
16. Iveland J, Martinelli L, Peretti J, Speck JS, Weisbuch C (2013) Direct measurement of Auger electrons emitted from a semiconductor light-emitting diode under electrical injection: identification of the dominant mechanism for efficiency droop. *Phys Rev Lett* 110(17):177406
17. Lu CF, Liao CH, Chen CY, Hsieh C, Kiang YW, Yang CC (2010) Reduction of the efficiency droop effect of a light-emitting diode through surface plasmon coupling. *Appl Phys Lett* 96(26):261104

18. Lin CH, Hsieh C, Tu CG, Kuo Y, Chen HS, Shih PY, Liao CH, Kiang YW, Yang CC, Lai CH, He GR, Yeh JH, Hsu TC (2014) Efficiency improvement of a vertical light-emitting diode through surface plasmon coupling and grating scattering. *Opt Express* 22(S3):A842–A856
19. Lin CH, Su CY, Kuo Y, Chen CH, Yao YF, Shih PY, Chen HS, Hsieh C, Kiang YW, Yang CC (2014) Further reduction of efficiency droop effect by adding a lower-index dielectric interlayer in a surface plasmon coupled blue light-emitting diode with surface metal nanoparticles. *Appl Phys Lett* 105(10):101106
20. Yeh DM, Huang CF, Chen CY, Lu YC, Yang CC (2008) Localized surface plasmon-induced emission enhancement of a green light-emitting diode. *Nanotechnology* 19(34):345201
21. Kuo Y, Chen HT, Chang WY, Chen HS, Yang CC, Kiang YW (2014) Enhancements of the emission and light extraction of a radiating dipole coupled with localized surface plasmon induced on a surface metal nanoparticle in a light-emitting device. *Opt Express* 22(S1):A155–A166
22. Sun G, Khurgin JB, Yang CC (2009) Impact of high-order surface plasmon modes of metal nanoparticles on enhancement of optical emission. *Appl Phys Lett* 95(17):171103
23. Lu YC, Chen YS, Tsai FJ, Wang JY, Lin CH, Chen CY, Kiang YW, Yang CC (2009) Improving emission enhancement in surface plasmon coupling with an InGaN/GaN quantum well by inserting a dielectric layer of low refractive index between metal and semiconductor. *Appl Phys Lett* 94(23):233113
24. Chen CY, Wang JY, Tsai FJ, Lu YC, Kiang YW, Yang CC (2009) Fabrication of sphere-like Au nanoparticles on substrate with laser irradiation and their polarized localized surface plasmon behaviors. *Opt Express* 17(16):14186–14198
25. Zhang S, Watson S, McKendry JJD, Massoubre D, Cogman A, Gu E, Henderson RK, Kelly AE, Dawson MD (2013) 1.5 Gbit/s multi-channel visible light communications using CMOS-controlled GaN-based LEDs. *J Lightwave Technol* 31(8):1211–1216
26. Tian P, McKendry JJD, Gong Z, Zhang S, Watson S, Zhu D, Watson IM, Gu E, Kelly AE, Humphreys CJ, Dawson MD (2014) Characteristics and applications of micro-pixelated GaN-based light emitting diodes on Si substrates. *J Appl Phys* 115(3):033112
27. Liao CL, Chang YF, Ho CL, Wu MC (2013) High-speed GaN-based blue light-emitting diodes with gallium-doped ZnO current spreading layer. *IEEE Electron Dev Lett* 34(2):611–613
28. Zhu S, Wang J, Yan J, Zhang Y, Pei Y, Si Z, Yang H, Zhao L, Liu Z, Li J (2014) Influence of AlGaIn electron blocking layer on modulation bandwidth of GaN-based light emitting diodes. *ECS Solid State Lett* 3(3):R11–R13
29. Huang CW, Tseng HY, Chen CY, Liao CH, Hsieh C, Chen KY, Lin HY, Chen HS, Jung YL, Kiang YW, Yang CC (2011) Fabrication of surface metal nanoparticles and their induced surface plasmon coupling with subsurface InGaIn/GaN wells. *Nanotechnology* 22(47):475201
30. Chen HS, Yao YF, Liao CH, Tu CG, Su CY, Chang WM, Kiang YW, Yang CC (2013) Light-emitting device with regularly patterned growth of an InGaIn/GaN quantum-well nanorod light-emitting diode array. *Opt Lett* 38(17):3370–3373
31. Khurgin JB, Sun G, Soref RA (2007) Enhancement of luminescence efficiency using surface plasmon polaritons: figures of merit. *J Opt Soc Am B* 24(8):1968–1980